

Cyclic behavior of wood-frame shear walls with vertical load and bending moment for mid-rise timber buildings

Paúl Orellana^{a,b,*}, Hernán Santa María^{a,b,c}, José Luis Almazán^{a,b}, Xavier Estrella^{a,b,d}

^a Department of Structural and Geotechnical Engineering, Pontificia Universidad Católica de Chile, Av. Vicuña Mackenna, Santiago 7820436, Chile

^b UC Center for Wood Innovation (CIM), Pontificia Universidad Católica de Chile, Av. Vicuña Mackenna, Santiago 7820436, Chile

^c Research Center for Integrated Disaster Risk Management (CIGIDEN), ANID/FONDAP/15110017, Av. Vicuña Mackenna, Santiago 7820436, Chile

^d University of Technology Sydney, 81 Broadway Street, Ultimo, NSW 2007, Australia

ARTICLE INFO

Keywords:

Mid-rise timber buildings
Wood-frame shear walls
Cyclic behavior
Shear strength
Shear stiffness
Sturdy end-studs
Strong hold-downs
Vertical load
Bending moment

ABSTRACT

In light wood-frame buildings, the gravitational and lateral force-resisting systems are composed of floor diaphragms and shear walls. During an earthquake, these walls are subjected to the simultaneous action of in-plane vertical force, shear force, and in-plane bending moment. In a mid-rise building, these internal forces can reach large magnitudes, especially on the lower stories, and could have an important influence on the lateral behavior of the walls. The historical use of light wood-frame construction has been in low-rise buildings. Consequently, few investigations have analyzed the effects of high gravitational forces or in-plane bending moment on the lateral behavior of wood shear walls designed for multi-story buildings. This paper presents an investigation of the cyclic lateral behavior of light wood-frame shear walls, designed for mid-rise buildings, subjected to large axial compressive load and in-plane bending moment. Eight wall specimens were experimentally tested with a cyclic lateral displacement protocol, a constant compressive load, and a cyclic in-plane bending moment. The effects of axial compressive load and in-plane bending moment were analyzed. Also, the wall length and the spacing of sheathing nails were varied to study the effects of these variables on the response. A numerical study was performed to show how these effects could influence the response of mid-rise timber buildings. An improvement in the lateral performance of the walls was observed compared to walls tested without compressive force nor bending moment, showing an increase in stiffness, load-carrying capacity, and dissipated energy.

1. Introduction

A construction-system widely used in timber buildings is the light wood-frame construction. This system allows the prefabrication of some structural elements, which reduces construction time and on-site fabrication errors. In a light wood-frame building, the gravitational and lateral force-resisting systems are composed of floor diaphragms and shear walls. There are two types of framing configurations for wood construction: the platform-frame, and the balloon-frame.

Fig. 1 shows a typical wood-frame shear wall for low-rise platform-frame buildings, which consists of a timber frame with vertical elements (studs) and horizontal elements (plates). These elements are connected at the ends with nails, generating connections with practically no bending stiffness [1]. To laterally brace the frame, structural wood-based panels are connected to the frame using metallic fasteners like nails or staples. The most frequently used panels are of oriented strand

board (OSB) and plywood. Depending on the design forces and required stiffness, the panels are installed on one or both sides of the wall. In the platform frame construction, the shear-walls have the inter-story height. Therefore, the vertical elements of the lateral-force-resisting system are interrupted by the horizontal diaphragms. To generate continuity in force-transfer and to prevent the overturning of walls, anchorage systems are installed through stories and to the foundation. Usually, that anchorage is provided by tension-carrying devices (e.g., hold-down anchors, continuous steel rods) at the end-studs and shear-carrying devices (e.g., shear bolts, plate shear connectors) at the base and top plates.

For lateral forces, wood-frame shear walls have a nonlinear force-deflection response and a cyclic hysteretic behavior, i.e., they can dissipate energy [2]. This energy dissipation-capacity is limited by a pinching effect. The same shear walls resist gravitational loads, then during an earthquake, these are subjected to the simultaneous action of in-plane axial force, in-plane shear force, and in-plane bending moment.

* Corresponding author.

E-mail address: pforellana@uc.cl (P. Orellana).

<https://doi.org/10.1016/j.engstruct.2021.112298>

Received 1 February 2020; Received in revised form 10 March 2021; Accepted 25 March 2021

Available online 29 April 2021

0141-0296/© 2021 Elsevier Ltd. All rights reserved.

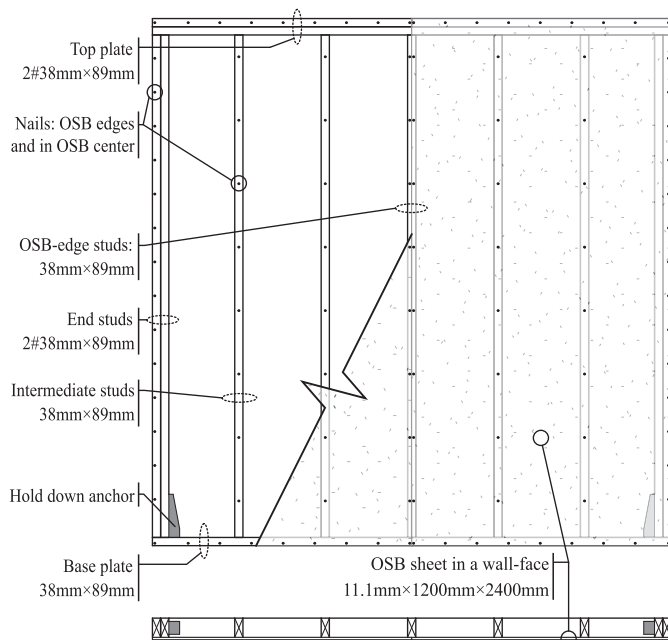


Fig. 1. Configuration of a 2400 mm long typical light wood-frame shear wall for low-rise buildings (adapted from [8]).

In a mid-rise building, these internal forces can reach large magnitudes compared to a 2-story house, especially on the walls of lower stories, and could influence the lateral response of the walls. The gravitational loads in a multi-story building generate high compressive forces in the lower walls, which require sturdy vertical studs. Also, lateral forces (i.e., seismic or wind forces) induce high tension forces in the end-studs. Therefore, strong anchorage systems (i.e., devices with dimensions larger than conventional ones and greater number and diameter of the bolts used in the connection) are needed to transfer these forces.

Another important issue in the seismic response of mid-rise buildings is the inter-story drift, which can produce damage in nonstructural components. Then, the lateral stiffness of wood-frame shear walls could control the multi-story building design. Also, an accurate estimation of the stiffness is needed to calculate the dynamic properties (i.e., natural periods and vibration modes) of the buildings. The historical use of the light wood-frame construction has been in low-rise residential and commercial buildings [3,4]. Therefore, most of the developments in research and regulations focus on wood shear walls for low-rise structures, e.g., [5,6,7]. Then, the traditional design methodologies for wood-frame shear walls do not consider the effects of high axial compressive forces and bending moments on the lateral behavior of the walls.

1.1. Experimental background

Many research projects have been conducted to study the seismic performance of timber buildings [3,5,9,10,11]. In those projects, an important part of the experimental component focused on the monotonic, cyclic, and dynamic behavior of wood shear walls. Literature reviews [2,6,12] summarized many publications about tests on wood shear walls for low-rise buildings. Generally, these tests were conducted applying lateral loading protocols, with no axial compressive force nor bending moment. For wood-frame shear walls, those studies showed that: the sheathing nail pattern has an important effect on the lateral load-carrying capacity, the observed failure modes were commonly associated with the panel to frame connections, and these connections are the main source of dissipation of energy.

Van de Lindt et al. [13] reported the results of shake table tests on a full-scale six-story wood-frame building. In the lower stories, many shear walls had sturdy studs and OSB sheathing panels on the two sides.

The building had a maximum average inter-story drift in the order of 2% and suffered only minor nonstructural damage due to an earthquake with a return period of 2500 years. However, these tests evaluated the whole system response. Therefore, the behavior of the wood-frame walls, as structural components, was not specifically observed.

Some researchers have studied the effects of vertical loads on the lateral behavior of light wood-frame shear walls. Dean and Shenton [14] and Johnston et al. [15] conducted static and cyclic tests in 2440×2440 mm common wood-frame shear walls. Those tests were conducted applying different levels of constant vertical compressive load, between 0 and 25 kN/m. The maximum applied vertical compressive force may represent the dead load on the first floor of a typical 2- to 4-story building. They concluded that, for walls with hold-downs, the vertical load increased the lateral load-carrying capacity by up to 50%, the initial lateral stiffness by up to 158%, and the energy dissipation by up to 100%. Hold-downs had little effect on the stiffness and energy dissipation capacity of a vertically loaded shear wall.

Salenikovitch and Payeur [8] tested common wood-frame shear walls of 2440×2440 mm and 4880×2440 mm, with and without hold-downs. The tests considered lateral cyclic loading and constant vertical compressive load between 0 and 16.3 kN/m. The maximum vertical compressive load applied corresponded to the force necessary to prevent overturning. An increase in the lateral load-carrying capacity was reported for walls without hold-downs. For fully anchored walls, there was no adverse influence of additional vertical gravity load on their lateral performance.

Grossi et al. [16,17] tested common wood-frame shear walls of 2500×2500 mm. These tests considered three levels of vertical compressive load, with values of 0, 10, and 20 kN/m, applied at the top plate of the walls. The authors reported that the increase of the vertical load led to an increase in the maximum lateral load-carrying capacity of 20% and 28%, and of the stiffness by 12% and 31%, for walls with vertical loads of 10 kN/m and 20 kN/m, respectively.

The above-cited investigations showed that there are beneficial effects of the compressive load on the structural response of wood-frame shear walls. However, these studies are limited to typical walls for low-rise structures, i.e., walls constructed with common sized elements and levels of vertical load smaller than the expected loads in mid-rise buildings.

Sadeghi Marzaleh et al. [18] studied walls with a configuration designed for mid-rise buildings, conducting three full-scale tests under a monotonic lateral loading protocol and combinations of vertical load and bending moment. The walls were 2500 mm long and 2800 mm high. The vertical elements of the frame consisted of two edge studs, one center stud, and two intermediate studs with sectional dimensions of 180×180 mm, 100×180 mm, and 60×180 mm, respectively, and the sheathing consisted of 15 mm thick OSB panels installed on both sides of the wall. The panels were connected to the frame using staples. The end-studs were anchored to the foundation using slotted-in steel plate connections with steel dowels, generating a rigid connection. In the three tests, a load of 60 kN was applied distributed on the top plate to represent the permanent load of the story supported by the wall. In addition, two concentrated loads were applied at the end-studs, representing the forces transferred by the walls of the upper floors. The concentrated loads had a magnitude of 15 kN, each one, for two tests with low vertical load; and 123 kN on each end-stud for a test with high vertical load. The level of the applied vertical load corresponds to residential or office 4-story buildings with timber-concrete composite slabs. The walls had ductile behavior, with the staples providing the main ductility to the system. Also, the applied increase in vertical load and the addition of bending moment marginally decreased the shear resistance and stiffness of the studied walls, which contradicts the works cited above. However, these observations may be due to differences in constructive details of the studied walls compared to conventional wood-frame walls. The configuration appears to be closer to a post-beam system braced with wood panels. Also, the monotonic tests do not

provide information about energy dissipation or cyclic behavior of the wood-frame walls. Such information is needed to adjust numerical models that could predict the dynamic response of shear walls (as structural components) and timber buildings (as structural systems).

To efficiently extend the use of wood-frame construction to mid-rise buildings there is a need to characterize the cyclic behavior of wood-frame shear walls with configurations specifically designed for mid-rise buildings, considering realistic loading conditions, i.e., taking account of the effects of axial vertical load and in-plane bending moment.

1.2. Objective

This paper presents an investigation conducted to characterize the cyclic lateral behavior of light wood-frame shear walls subjected to high axial compressive load (CL) and in-plane bending moment (BM). The studied walls had a configuration suitable to be used in the lower stories of mid-rise platform-frame timber buildings, up to 6-story high.

The lateral cyclic force–deflection response of the walls was investigated through full-scale tests. The applied axial compressive load was greater than the vertical loads applied in most of the previous experimental studies reported in the literature. The effects of axial CL and in-plane BM on the behavior of the shear walls were analyzed and a numerical study was performed to show how these effects could influence the response of mid-rise timber buildings.

2. Materials and methodology

2.1. Test specimens

Eight full-scale wood-frame shear wall specimens were tested. The specimens were 2470 mm high with three different lengths: 1200 mm, 2400 mm, and 3600 mm. The labeling (ID) of the test specimens was done through an alphanumeric code that starts with the letter A followed by the length of the wall in centimeters, the panel-edge nail spacing in centimeters, and the sample number (for repetitions of the same configuration). The wall configuration is shown in Fig. 2. The framing members of the walls consisted of MGP10 graded Chilean

radiata pine (*pinus radiata*) elements, according to the Chilean national regulations NCh1198 [19], with cross-sectional dimensions of 2" × 6" (36 × 138 mm). The sturdy vertical end-studs were built with five 2" × 6" (36 × 138 mm) elements attached with nails and glue. The intermediate vertical studs were single 2" × 6" elements in the center of the panels and two 2" × 6" elements (nailed and glued) in the edges of the panels. Two 2" × 6" elements (nailed and glued) were placed as bottom and top plates of the walls. APA OSB rated 7/16" panels (11.1 mm thick) were used for sheathing on both faces of the wall. Each 1200 mm by 2400 mm sheathing panel was connected to the frame with Ø3 mm × 70 mm helical nails spaced 100 mm or 50 mm in the panel edges and spaced 200 mm in the center of the panels. Simpson-StrongTie HD12 hold-down anchors were placed at the top and bottom in the inner face of the end-studs. The hold-downs were connected with four Ø1" × 10" bolts to the end-studs and with a Ø1-1/8" × 10" bolt to a foundation steel beam and to a loading steel beam on top of the wall. To control the slip of the wall, Ø1" shear bolts were installed through the bottom and top-plates between the vertical studs.

2.2. Test set-up

Fig. 3 shows a photograph and a schematic view of the test set-up. To facilitate the application of the loads in the laboratory, the test set-up was designed with the wall-plane of the sample oriented in horizontal position. The wall was anchored to a foundation steel beam at the base. The foundation-beam displacement was restricted by a reinforced concrete reaction wall and steel reaction elements connected to a reinforced concrete strong floor. A lateral displacement-controlled loading protocol was applied by a hydraulic actuator through a steel beam (load-beam) connected to the top-plate of the wall. On the load-beam, two hydraulic actuators applied force-controlled loading protocols to produce a constant compressive load and a cyclic in-plane bending moment. The compressive-force actuators had rollers at the contact with the load-beam to allow the lateral displacement of the wall specimen during cyclic excitation.

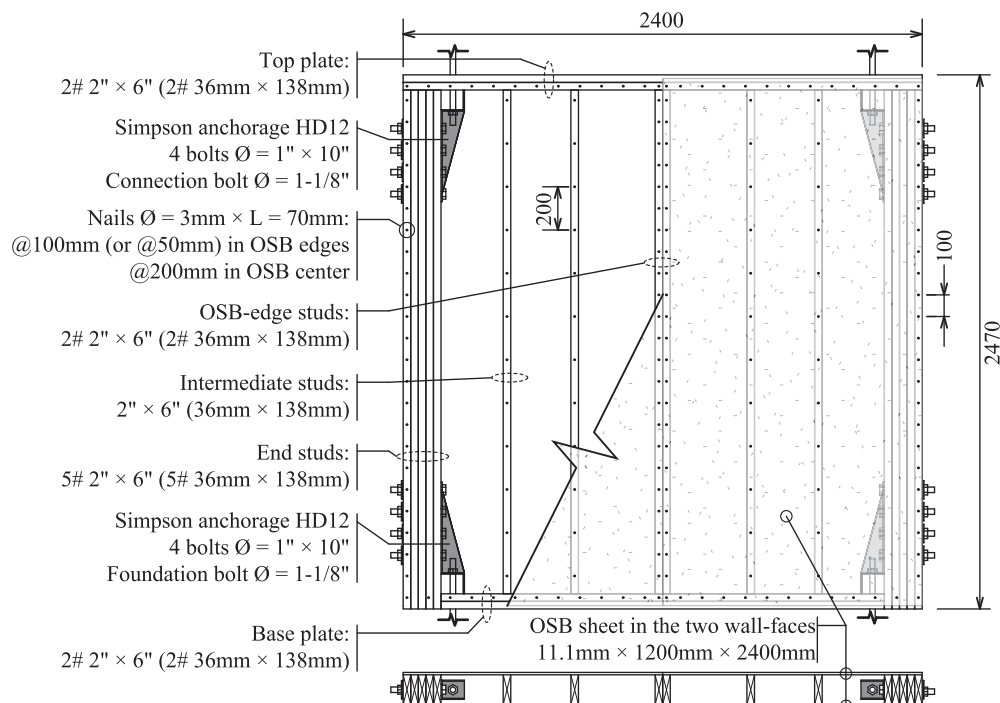
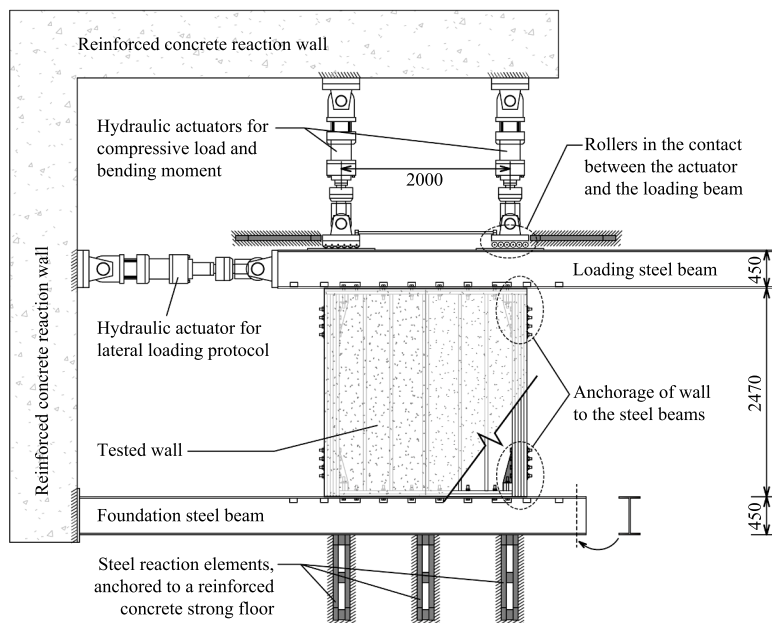


Fig. 2. Configuration of a 2400 mm long test specimen (dimensions in mm).



(a) Photograph (of a 1200 mm long wall).



(b) Schematic top view (of a 2400 mm long wall, dimensions in mm).

Fig. 3. Test set-up.

2.3. Test instrumentation

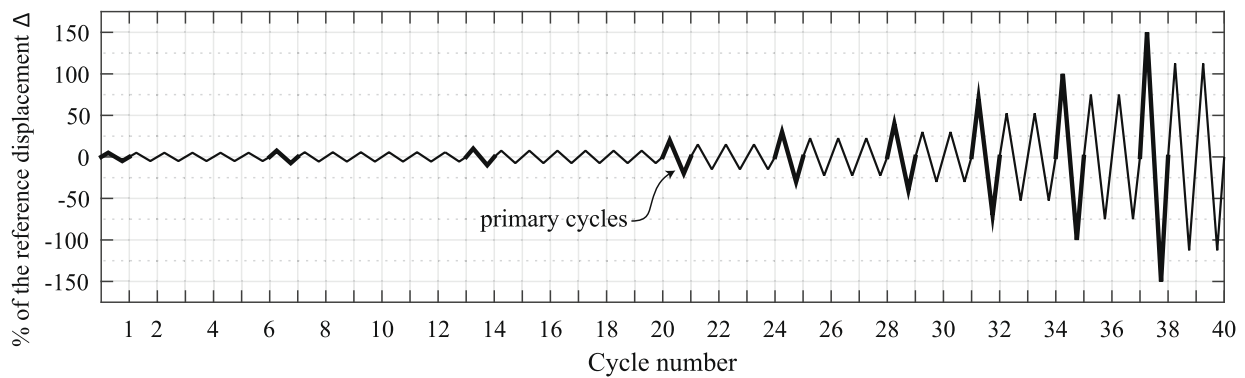
The displacement and force of the lateral loading actuator were measured during the test (i.e., the lateral displacement of the load-beam). The instrumentation included displacement transducers to measure the relative slip between the wall and both steel beams. Then, the lateral deflection of the walls was calculated as the difference between the lateral displacement of the load-beam and the total slip of the wall-plates (bottom and top plates) relative to the steel beams (obtaining the lateral displacement of the top plate relative to the base plate).

Displacement transducers were placed at the wall vertices to measure the uplift between the end-studs and the steel beams. A displacement transducer measured the deformation of the diagonal of the wall. Also, there were transducers to measure the relative slip between the hold down anchorage and the studs, the axial deformation of the studs, and the in-plane rigid-body motions of the load-beam.

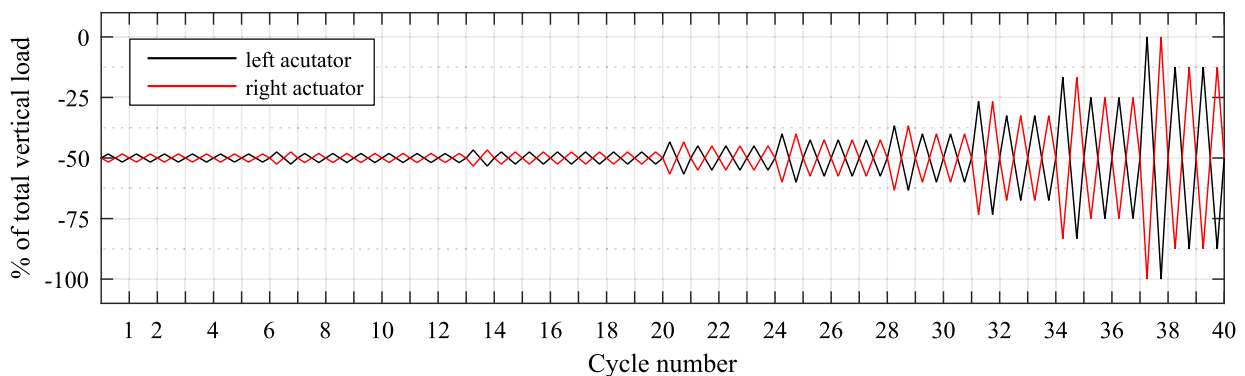
2.4. Test procedure

The walls were subjected to lateral cyclic displacement and simultaneous constant axial compressive load and cyclic in-plane bending moment, which better represent the actual forces in a shear wall. The displacement-controlled actuator applied the CUREE protocol [20,21] with the amplitude of displacements calibrated according to the results of tests reported by Guíñez et al. [22] for walls with the same configuration but tested without vertical load nor bending moment. Fig. 4(a) shows the displacement protocol, Δ is a reference displacement obtained from previous tests [22]. The value of Δ did not exceed 0.025 times the wall height [21].

The total compressive force applied by the two actuators represents a constant uniformly distributed load of approximately 75 kN/m applied on the top of the walls. This load was obtained from the structural design of a 6-story wood-frame building following the guidelines of the NCh433 standard [23]. Regarding vertical loads, in such design, a live load of 2 kN/m² was considered, and dead loads were calculated based on the



(a) CUREE displacement protocol for the lateral-loading actuator.



(b) Compressive loading protocol for each actuator.

Fig. 4. Loading protocols.

self-weight of structural elements and timber floors (2–2.5 kN/m², approximately). The structural elements taken into account for computing dead loads were: (1) shear walls (timber studs, OSB panels, anchoring devices, and non-structural sheathing panels), and (2) the flooring system (chords, collectors, beams, blocking, sheathing panels, and acoustic and thermal insulation). The flooring system selected for this case study was a common blocked wood-frame solution with a 50 mm thick concrete layer on top. The latter had mainly a non-structural purpose (acoustic and thermal insulation) and was not coupled to the timber flooring. The vertical load for each wall was calculated based on its tributary area determined from the floor-plan distribution. For the ground floor, vertical loads on walls ranged from 59 to 89 kN/m. Therefore, an average value of 75 kN/m was selected for this research to be consistent with the expected forces in the lower stories of multi-story wood-frame buildings.

The force applied by each actuator varied such that the bending moment generated was proportional to the displacement applied by the lateral-loading actuator, but the vertical load was constant. A reference bending moment was defined as the moment that results when one actuator applies the total compressive load while the other one applies zero force. This reference bending moment was achieved for the lateral displacement at the maximum lateral force obtained in a corresponding cyclic test of a wall without compressive load nor bending moment [22]. Fig. 4(b) shows the force protocol for each actuator. Also, there was an additional bending moment due to the eccentricity of the lateral-loading actuator (acting on the longitudinal axis of the load-beam) relative to the top-plate of the wall. This additional bending moment depended on the lateral force. It could not be controlled due that the lateral excitation having been a displacement-controlled loading. The loads applied on the test specimens aimed to represent the loading-state of a shear wall which

is part of a building dynamically responding in its first mode of vibration, in which all the seismic mass displaces in the same direction in each instant of time.

2.5. Wall performance evaluation

The evaluation of the performance of the tested walls was made according to the methodology presented in [21]. The envelope curve is defined as the curve that contains the peak forces from the primary cycles (cycle with amplitude greater than the subsequent ones) of each phase of the displacement protocol. Fig. 5(a) shows an example of the hysteresis loops and the envelope curves associated. P_{peak} is the maximum absolute value of force in the envelope curve. An average envelope curve is obtained by averaging the absolute values of force and displacement of the corresponding positive and negative envelope curves, as shown in Fig. 5(b). The ideal equivalent energy elastic-plastic (EEEP) curve circumscribes an area equal to the area enclosed by the average envelope curve between the origin, the ultimate displacement, and the displacement axis (Fig. 5c). The ultimate displacement Δ_u is defined as the displacement associated with the ultimate force P_u , which corresponds to the data point, in the envelope curve, with the force equal to or greater than $|0.8P_{peak}|$. The elastic stiffness of the EEEP curve was calculated as the secant stiffness in the average envelope curve at the force value of $0.4P_{peak}$.

In cyclic loading tests, the equivalent viscous damping (EVD) is a commonly used metric to evaluate the damping of structural components [24]. The EVD is calculated by equating the energy dissipated in a loading cycle of the system and an equivalent viscous system under harmonic excitation. The energy dissipated by the system, E_d , is the area within the hysteresis loop. For a specific loop, the EVD is calculated as:

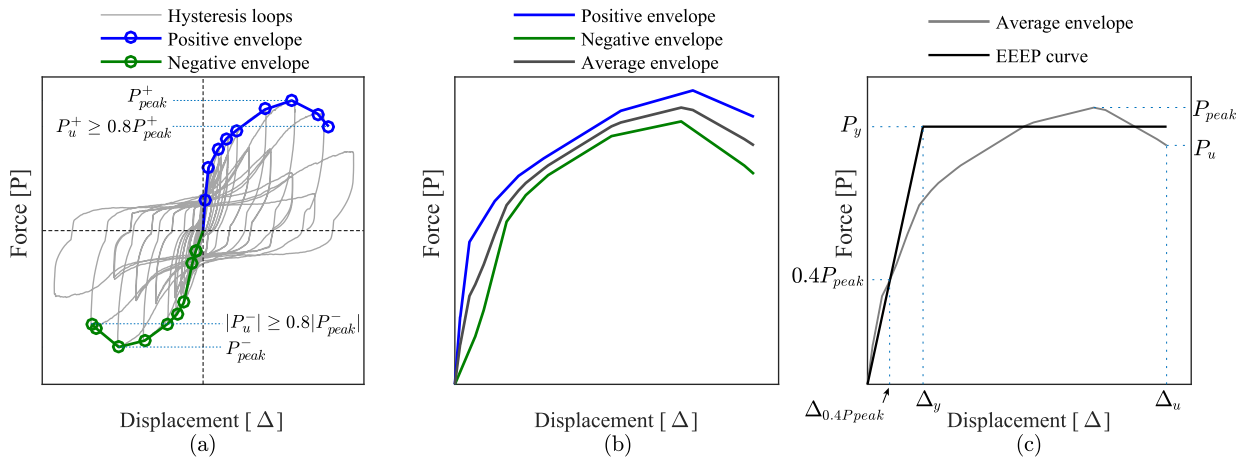


Fig. 5. Envelope curves and equivalent energy elastic-plastic (EEEE) curve [21].

$$\xi_e = \frac{1}{4\pi} \frac{E_d}{E_{so}} \quad (1)$$

where E_{so} is the maximum loop's elastic strain energy calculated using an effective stiffness, K_{eff} , associated with the maximum loop's displacement Δ_{max} (Fig. 6):

$$E_{so} = \frac{1}{2} K_{eff} \Delta_{max}^2 \quad (2)$$

$$K_{eff} = \frac{P^+ - P^-}{\Delta^+ - \Delta^-} \quad (3)$$

where P^+ is the force corresponding to the absolute maximum positive displacement, Δ^+ , and P^- is the force corresponding to the absolute maximum negative displacement, Δ^- .

The EVD was calculated using the shear deformation of the walls, representing the dissipation capacity of the wall despite the anchorage system.

2.6. Effects of compressive load and bending moment on wall behavior

To evaluate the simultaneous effects of the compressive load and bending moment, the responses of the walls were compared with the published results of a previous set of tests [22] for walls with the same configurations but tested without CL nor BM. In this paper, to identify those walls the alphanumeric label (ID) starts with the letter C (as originally published in [22]) followed by the length (in centimeters), the panel-edge nail spacing (in centimeters), and the sample number.

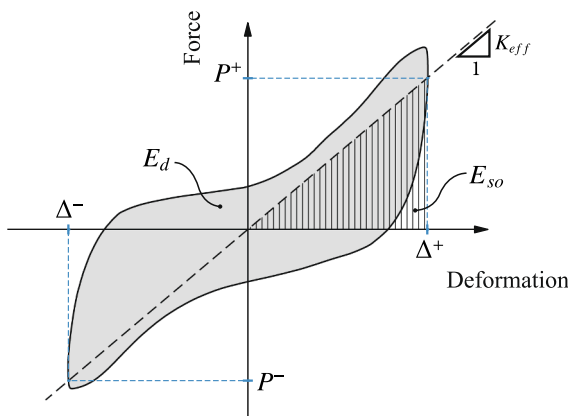


Fig. 6. An arbitrary hysteresis loop. Equivalent viscous damping definition [24].

Therefore, to distinguish between the two sets of tests, the walls reported here are identified as A-walls and the walls reported in [22] are identified as C-walls.

2.7. Numerical analysis of a 5-story building

It is expected that any change in the performance of wood-frame walls due to high CL and BM has a relevant influence on the seismic behavior of mid-rise buildings. To evaluate such influence, static and dynamic analyses were performed for a 5-story wood-frame building designed using the current Chilean seismic code (NCh433) [23]. The height of the building was defined to comply with the NCh433 code, which allows using an equivalent lateral force analysis to calculate the seismic design forces for buildings up to 5-stories. The building represents a typical 4-apartment private building with 490 m² of living space and irregular perimeter, placed on seismic zone 3 and soil type A as defined in [23]. The floor plan is shown in Fig. 7.

The structural design of the building was made according to the Chilean seismic regulations NCh433 [23] and the Special Design Provisions for Wind and Seismic (SDPWS) [25]. As explained in section 2.4, a live load L of 2 kN/m² was considered, and dead loads D were calculated from the self-weight of structural elements and timber floors (2 to 2.5 kN/m²). Then, the seismic mass of each story was calculated as $D + 0.25L$ [23]. The seismic lateral design forces were calculated by a

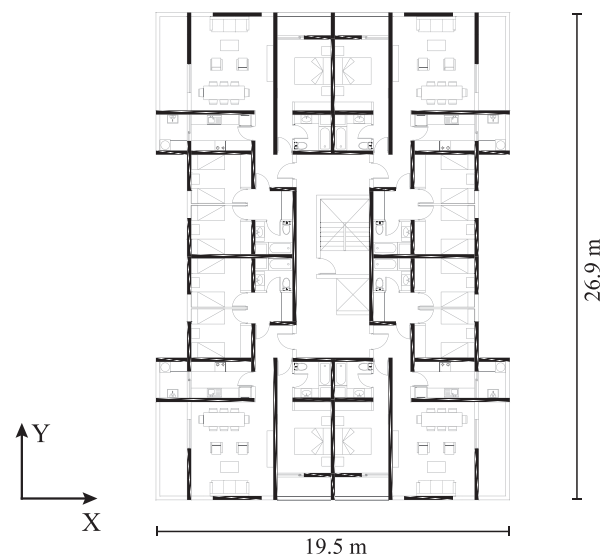


Fig. 7. Floor plan of the analyzed 5-story timber building.

static analysis on a linear model of the structure. The design base shear was obtained from the code-defined acceleration spectrum [23], where accidental torsion effects were also included. To calculate the base shear, the period of the structure was computed using the expression proposed by Nassani [26]. The vertical distribution of the lateral forces followed the guidelines in Section 6.2.5. of the NCh433 standard [23]. The shear force for each wall of the floor was computed proportionally to its stiffness. Finally, the design values of the walls were obtained from the SDPWS standard [25], and the properties of the materials from the Chilean NCh1198 code [19].

To properly study the effects of the compressive load and bending moment, two nonlinear models were developed for the same building: (1) one that considers the effects of the vertical load in lower stories –identified as A-model in this paper– and (2) one that does not –identified as C-model–. As the initial step when creating the first model, the lateral response of the walls tested in this study was reproduced employing the CASHEW (cyclic analysis of shear walls) model proposed by Folz and Filiatrault [27]. The non-linearity in the models was introduced through the panel-to-frame connections, whose hysteretic behavior was modeled using the MSTEWE (modified Stewart) model [27]. The parameters of the model were empirically fitted to match the overall experimental response of each wall. The calibrated model for the specimen A240-10-01 is shown in Fig. 8. To model the entire building, the simplified 3D approach proposed by Pei and van de Lindt [28] was employed. In this approach, each wood-frame wall is represented by three unidirectional springs: one nonlinear horizontal spring to model the shear behavior of the wall, and two bi-linear vertical springs to capture the combined stiffness of hold-downs, studs, continuous steel rods, and any special fastener element. Fig. 9 shows a schematic of the shear-wall element into the structural 3D model of the building. The MSTEWE model was employed to represent the hysteretic response of the horizontal springs, whose parameters for the two first stories were obtained from the CASHEW models previously discussed (i.e., correspond to the A-walls). For the three upper stories, the MSTEWE parameters were obtained from experimental results of wood-frame walls tested only under lateral loading protocols [22] (C-walls), based on the data provided by Estrella et al. [29]. The rationale for this assumption is based on the fact that the effect of the vertical load on the walls of the upper stories is not as significant as the effect on the walls of the lower stories, as previous research has shown [14,15]. A similar approach was followed for the C-model that does not consider the effects of the vertical load, therefore the horizontal springs in all five stories were modeled based on walls tested only under lateral loading protocols.

Static pushover analyses were conducted employing both models. The lateral force was applied following a modal adaptive distribution over the height of the structure until the base shear fell by 40%. Both

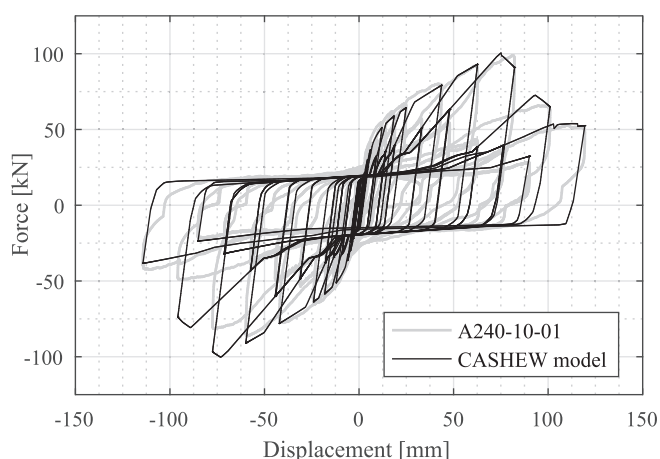


Fig. 8. Test results versus model predictions for specimen A240-10-01.

directions (X-axis and Y-axis) were analyzed separately.

A bi-directional time-history analysis was also conducted to study the effects of the vertical loads on the dynamic response of the building. The ground motion employed as dynamic input was recorded during the 8.8 Mw Maule earthquake (Angol station) in Chile [30]. The peak ground accelerations of the record are 0.70 g and 0.93 g in the X and Y direction, respectively.

To analyze the response of both models when facing several earthquakes with different dynamic properties, an incremental dynamic analysis (IDA) [31] was conducted employing a set of 26 pairs of ground motions [32] recorded from different events in the last 30 years. Each pair of ground motions was applied twice to each model, once with the records oriented along the principal direction, and then again with the records rotated 90 degrees (a total of 52 IDA analysis for each model). The 5% damped spectral acceleration associated with the fundamental period was used as intensity measure and the maximum inter-story drift as damage measure. A maximum inter-story drift of 3% was used as collapse capacity limit.

3. Results and discussion

3.1. Performance of the tested shear walls

The main failure modes observed in the tested walls were: a combination of shear- and bending-failure of the nails in panel edges (Fig. 10a); local crushing of the panel-wood in the nail contact area, with some nails crossed the panel (Fig. 10b); nails pulled out from the frame and local permanent deformation of the frame-wood in the nail contact area; and out of plane buckling of the panels for large displacements (Fig. 10c). The buckling of the panels was caused by the contact between the panels and the steel beams at large displacements. There was no damage observed on the frame timber elements or the anchorage devices.

Fig. 11 shows the hysteresis curves for the eight tested walls. The hysteresis curves were constructed with the total lateral displacement of the top-plate relative to the base-plate and were used to define the envelope and the EEEP curves. The shape of the hysteresis curves shows a complex nonlinear response and hysteresis loops with pinched area, similar to those reported in previous studies [15,22,33,34] for wood-frame shear walls. The observed failure modes suggest that the cyclic behavior of the panel to frame nailed connections has the main influence on the global lateral behavior of the shear walls.

Table 1 presents a summary of the test results, including the maximum absolute force measured during the tests, P_{max} ; the peak force, P_{peak} , of the average envelope curve; the parameters of the EEEP curve, K_0 , Δ_y , Δ_u ; the ductility ratio, $\mu = \Delta_u/\Delta_y$; and the drift ratio at a force of $0.4P_{peak}$, $\delta_{40} = \Delta_{0.4P_{peak}}/H$, with $H =$ wall height. The displacement for which the measured overturning moment was equal to the resisting moment, Δ_R , was used to calculate the drift ratio associated with the start of the uplift of the end-studs, $\delta_R = \Delta_R/H$. The aforementioned parameters were calculated for the hysteresis loops of the total lateral displacement of the top plate relative to the base plate. A representative value for the EVD, ξ_E , is reported in the results; ξ_E corresponds to the 10% percentile of the set of EVD values calculated for all the hysteresis loops for a tested wall, considering only the shear deformation (i.e., despite the overturning component of displacement).

The results presented in Table 1 show the effects of the wall length and panel edge nail spacing on the analyzed indicators of performance. The maximum load-carrying capacity (P_{max} and P_{peak}) increases as the wall length increases or as the nail spacing decreases. The elastic stiffness, K_0 , increases as the wall length increases, but no effect of the nail spacing is observed on this parameter. The representative EVD, ξ_E , appears to decrease with an increase in wall length, but it is not a clear trend; no dependence is observed with the nail spacing. Regarding the ductility ratio μ , no clear trend is observed with respect to the effect of

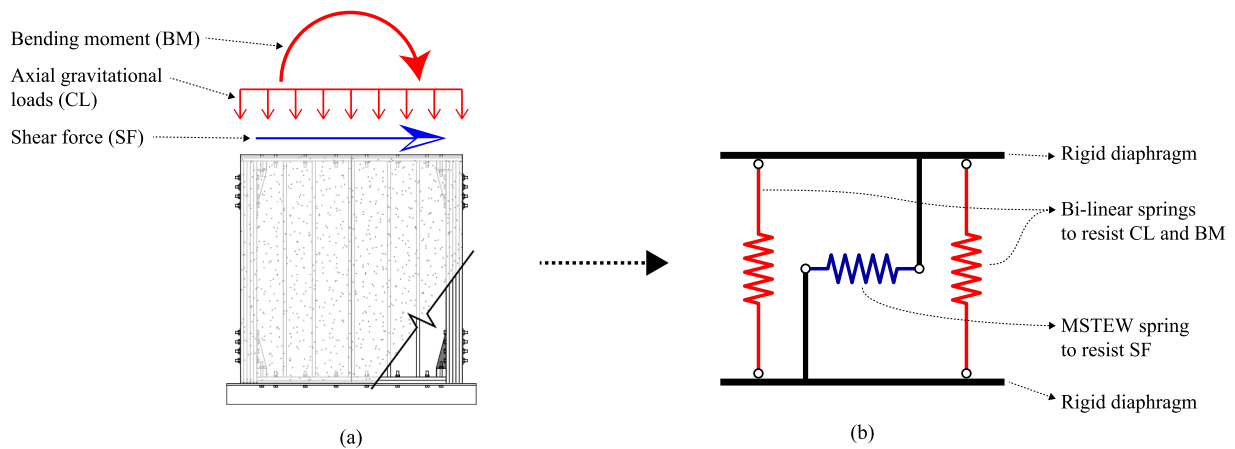


Fig. 9. Schema of the shear-wall element into the structural 3D model of the building [28]. (a) Internal forces acting on a wall. (b) Shear-wall element, springs to resist the internal forces.



(a) Shear- and bending-failure of the nails in panel (b) Panel crushing due to the progressive damage of edges.



(c) Panel buckling due to the contact between the panels and the steel beams at large displacements.

Fig. 10. Failure modes.

the wall length, as similarly was observed in previous tests of walls, with the same configurations, but tested without CL [22]. On the other hand, the ductility ratio decreased and the ultimate displacement increased as the nail spacing decreased. This is explained because the increase of strength, due to the decrease in nail spacing, is much larger than the corresponding increase in the value of Δ_u . Comparing the reported drift parameters; for all cases, except for the A120-05-01 wall, the drift which initiated the uplift, δ_R , is greater than the drift δ_{40} for which the elastic stiffness was defined. Consequently, the elastic stiffness of the A-walls

was greater than the elastic stiffness of walls tested without CL [22] for which the uplift initiated from the beginning of the experiment.

Fig. 12 shows the unit force envelope curves for the eight tests. In these curves, the lateral forces are normalized by the wall length (P/L , with L = wall length). The curves are clustered by nail spacing. The maximum unit load-carrying capacity and the ultimate unit force were achieved for drift levels between 2% and 3.5% for the walls with panel-edge nails spaced 100 mm, and for drift levels between 2% and 4% for the walls with panel-edge nails spaced 50 mm. In Fig. 12(a) for a specific

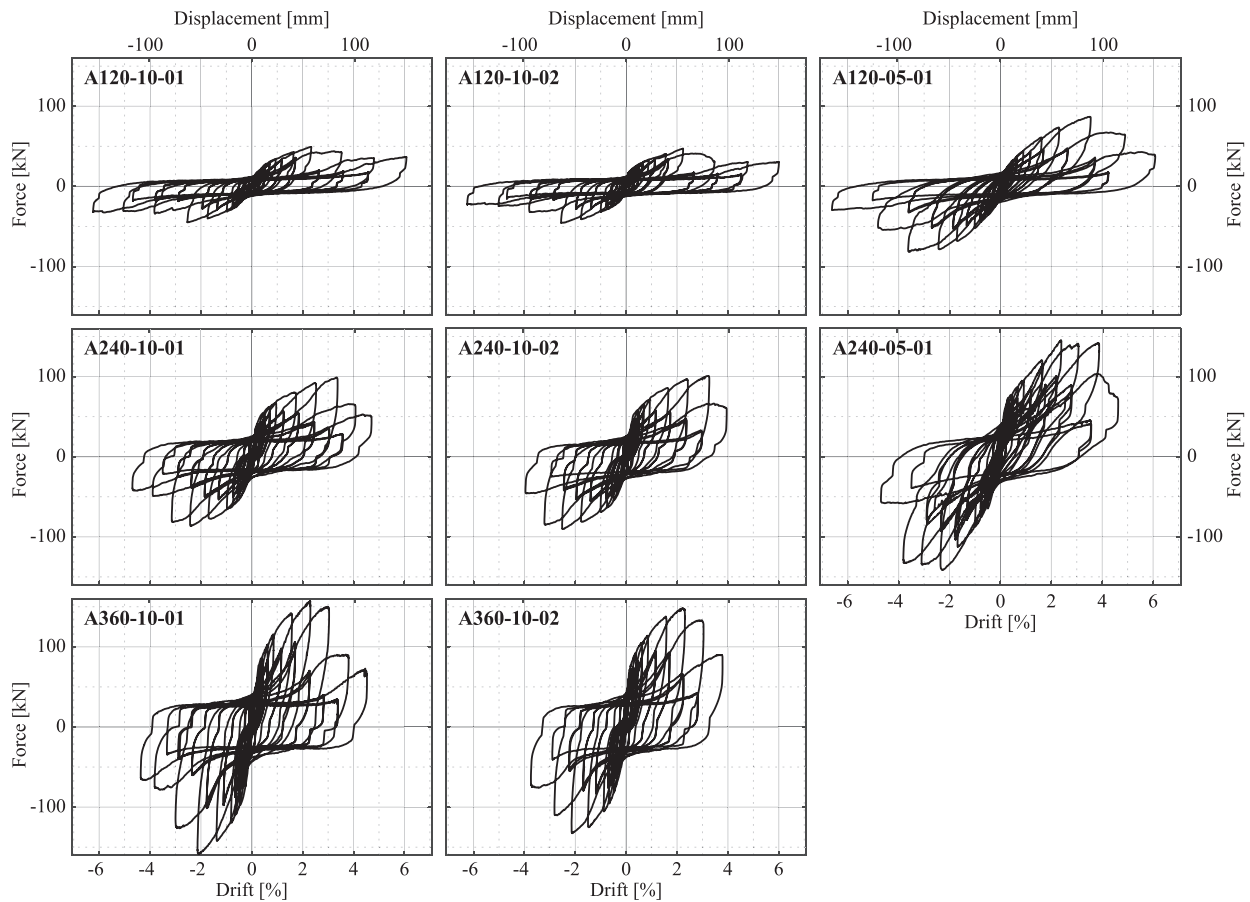


Fig. 11. Force-displacement response curves for lateral displacement of the top plate relative to the base plate.

Table 1

Results from the cyclic tests of walls with vertical load and bending moment.

Tested wall	P_{max} [kN]	P_{peak} [kN]	K_0 [kN/mm]	δ_{40} [%]	δ_R [%]	ξ_E [-]	Δ_y [mm]	Δ_u [mm]	μ [-]
A120-10-01	49.2	46.3	2.30	0.33	0.34	0.22	17	89	5.1
A120-10-02	47.0	45.4	3.63	0.20	0.24	0.22	10	64	6.3
A120-05-01	86.9	84.2	2.84	0.48	0.17	0.22	25	104	4.1
A240-10-01	98.9	89.3	6.87	0.21	0.92	0.21	11	84	7.4
A240-10-02	101	93.8	6.97	0.22	0.84	0.12	12	82	7.0
A240-05-01	145	143	6.49	0.36	0.61	0.22	19	93	4.9
A360-10-01	159	156	10.5	0.24	1.79	0.10	13	70	5.4
A360-10-02	148	140	9.64	0.23	2.17	0.16	13	69	5.4

wall length, the specimens with nail-spacing of 50 mm had greater initial unit stiffness than walls with nail-spacing of 100 mm. Table 2 presents the average values of the maximum force per unit length, $p_{max} = P_{max}/L$, and the elastic stiffness per unit length, $k_0 = K_0/L$. The maximum unit force increases as the nail spacing decreases, while it does not depend on the wall length. The unit elastic stiffness is independent of the nail spacing and appears to slightly increase with an increase in wall length, but there is no clear trend.

The nominal unit lateral load-carrying capacity according to the SDPWS provisions [25], for walls equivalent to the analyzed walls, is 23.1 kN/m for panel-edge nails spaced 100 mm (4") and 39.1 kN/m for panel-edge nails spaced 50 mm (2"). These values were obtained from table 4.3A of the SDPWS [25] considering 11 mm (7/16") thick panels and common 8d nails. Comparing these values with the corresponding values of Table 2, the unit shear capacity of the tested walls reaches between 1.55- and 1.85-times the nominal shear capacity estimated according to the SDPWS [25]. These design provisions present an

equation to estimate the elastic deflection of the shear walls (Eq. (4), equation 4.3-1 in [25]). In equation (4), the first term takes into account the bending deflection of the wall, the second term represents the shear deformation through an apparent shear stiffness, G_a , that includes the panel shear deformation and the fastener slip; and the third term considers the anchorage deformation.

$$\Delta_{sw} = \frac{8pH^3}{EAL} + \frac{pH}{nG_a} + \frac{H\Delta_a}{L} \quad (4)$$

where Δ_{sw} is the lateral deflection of the wall, $p = P/L$ is the unit lateral force that induces this deflection (with $L =$ wall length), H is the height of the wall, E and A are the elastic module and the area of the transversal section of the end-stud, n is the number of wall faces sheathed with panels ($n = 2$ for the analyzed walls), G_a is the apparent shear stiffness of the panels, which includes the shear deformation of the panels and the slip of the connection, and Δ_a is the deformation of the anchorage device induced by the unit force p .

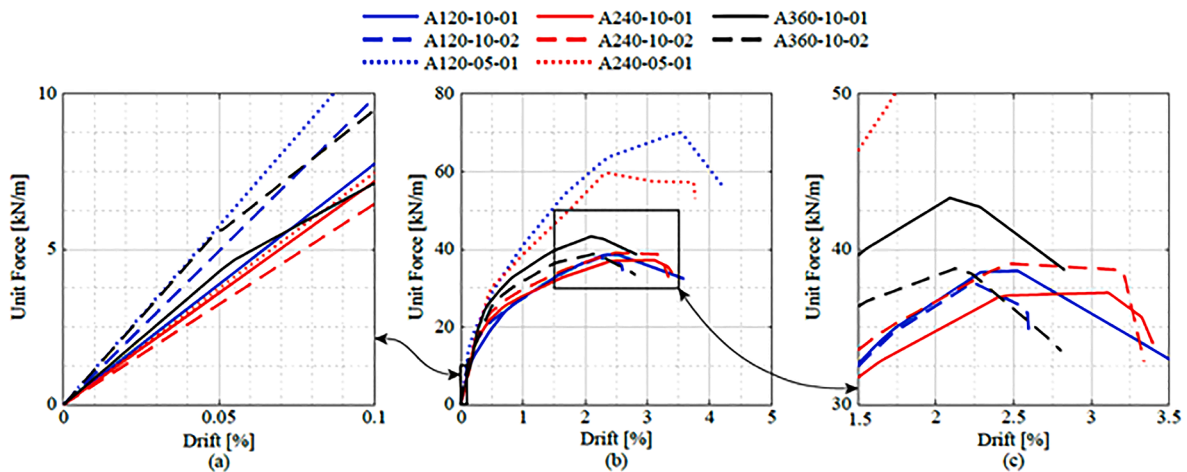


Fig. 12. Envelope curves for the tested walls with unit lateral force (force divided by wall length).

Table 2

Unit load-carrying capacity, unit stiffness, equivalent viscous damping, and ductility ratio of walls for cyclic tests with vertical load and bending moment (A-walls), and cyclic tests without vertical load nor bending moment (C-walls) [22].

Wall Configuration[1]	p_{max} [kN/m]			k_0 [kN/mm/m]			ξ_E [-]			μ [-]		
	A	C	A/C	A	C	A/C	A	C	A/C	A	C	A/C
120-10	40.1	37.0	1.08	2.5	0.9	2.91	0.22	0.09	2.56	5.66	3.15	1.80
120-05	72.4	47.1	1.54	2.4	1.0	2.30	0.22	0.10	2.17	4.10	3.35	1.22
240-10	41.6	31.8	1.31	2.9	1.1	2.53	0.16	0.10	1.65	7.23	3.85	1.88
240-05	60.5	37.2	1.63	2.7	1.3	2.03	0.22	0.09	2.48	4.89	3.70	1.32
360-10	42.6	33.6	1.27	2.8	1.2	2.30	0.13	0.10	1.36	5.37	3.55	1.51

[1] For tests with the same configuration, the table shows the average value for each parameter.

An estimation of the initial elastic unit stiffness can be calculated based on Eq. (4). To compare the SDPWS-based estimation of the stiffness with the stiffness of the tested walls, the anchorage deformation component of the equation was excluded. This assumption is based on the effect of the vertical load that restrains the uplift of end-studs for small displacements and therefore avoids the anchorage deformation. Then, the elastic unit stiffness, k_{sw} , is calculated as:

$$k_{sw} = \frac{1}{\frac{8H^3}{EAL^2} + \frac{H}{nG_aL}} \quad (5)$$

Considering 11 mm (7/16") thick panels and common 8d nails in table 4.3A of the SDPWS [25], the apparent shear stiffness is $G_a = 3.69$ kN/mm for walls with panel-edge nails spaced 100 mm (4") and $G_a = 7.02$ kN/mm for walls with panel-edge nails spaced 50 mm (2"). Considering an elastic module of $E = 10$ GPa for the end-studs (according to NCh1198 provisions [19]), the unit elastic stiffness, k_0 , of the tested walls (see Table 2) is 1.02- to 1.85-times the SDPWS-based estimation (Eq. (5)).

3.2. Effects of compressive load and bending moment on wall behavior

Table 2 presents the values of the maximum force per unit length, p_{max} , the values of the elastic stiffness per unit length, k_0 , the representative equivalent viscous damping, ξ_E , and the ductility ratio, μ , for the walls tested with axial compressive load and bending moment (A-walls) and without axial compressive load nor bending moment (C-walls). The A-walls have larger response parameters than the C-walls [22]. The unit elastic stiffness are 2- to 2.9-times the stiffness of C-walls, and the increase in unit stiffness is smaller as the wall length increases. This is due to the compressive load that restrains the uplift of the wall and, therefore, reduces the overturning component of the lateral displacement. This is confirmed by observing that the uplift-drift, δ_R , is larger than the drift δ_{40} for which the elastic stiffness was defined (see

Table 1). Table 2 shows that the resistance increases between 8 and 63%; the greater increase is for the walls with nails spaced 50 mm in the panel edges. The ductility ratios of the A-walls are 1.2- to 1.9-times larger than those of the C-walls. The increase is larger in walls with nail spacing of 100 mm in the panel edges.

To compare the shape of the hysteresis loops of the A-walls and C-walls, the lateral forces in the curves of Fig. 13 were normalized by the maximum force measured during each test. The general shape of the hysteresis loops is similar for the A-walls and C-walls. However, observing the loading and unloading paths of the hysteresis loops, the pinched response of the A-walls has a greater amplitude between the force-axis intercept points than that of the C-walls (as a percentage of the maximum lateral load-carrying capacity). This indicates that the hysteresis loops for the A-walls describe a larger area than those of the C-walls, showing a greater capacity to dissipate energy, which is consistent with the larger equivalent damping ratio observed in A-walls (see Table 2). This agrees with the observations made by Johnston et al. [15] for walls tested with various levels of vertical load, but without bending moment. Observing the post-peak behavior in the hysteresis curves of the A-walls, the secondary post-peak loops have a box-shape. This shape is similar to the hysteretic behavior of a frictional damper, which suggests that the improvement in the dissipation capacity of the A-walls, compared to the C-walls, may be due to a frictional phenomenon induced (or intensified) by the CL or the BM.

For the A-walls in the post-peak response loops, at the force-axis intercept points, the loading path is practically horizontal (see Fig. 13). The measured force-intercept values are approximately 10% of the total vertical load applied on the top plate (ranging from 8.8% to 11.7% with an average of 9.9%). In the well-known Coulomb friction model, the friction forces are proportional to the normal forces and the coefficient of friction between the surfaces with slip-contact. Then, it is reasonable to expect that the CL (or BM) could increase those forces. In the initial cycles (i.e., small displacements) energy dissipation occurs

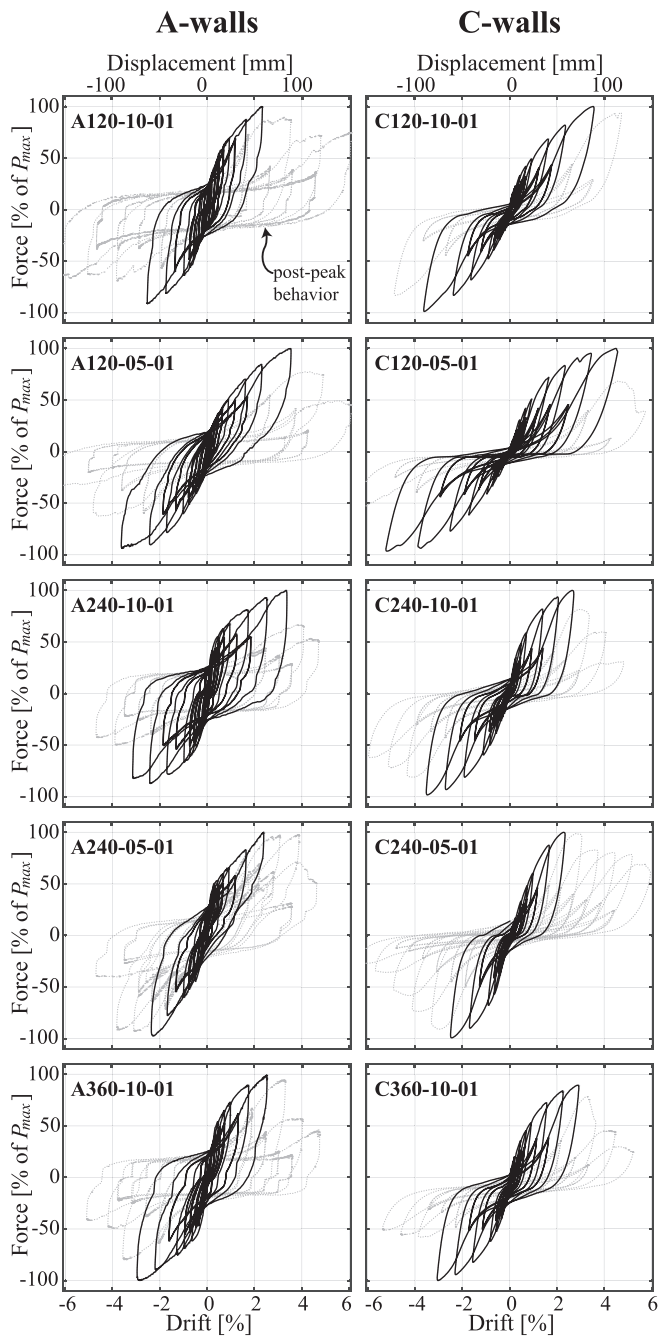


Fig. 13. Comparison of the shape of the hysteresis curves of walls tested with compressive load and bending moment (A-walls) and walls tested without compressive load nor bending moment (C-walls) [22].

mainly due to the panel-to-frame friction [35]. But in post-peak behavior, it is reasonable to suppose that the generated gap between the panels and the frame causes the panel-to-frame friction to be negligible. Other possible sources of friction could be in the interaction between the frame members or between the frame and the anchorage devices. The measured data show small slip between anchorages and end-studs, which suggests that there is no frictional dissipation on that contact.

As can be seen in Fig. 2, the sturdy end-studs were fabricated with 5 timber elements attached with nails and adhesive. Then, the relative slip between the individual timber elements that form the end-studs can be a source of dissipation due to the hysteretic behavior of the nailed connection and viscous dissipation in the adhesive material. Another

possible source of dissipation is the plastic deformation of the anchorage bolts, however, no permanent deformation was observed in those elements.

Fig. 14 shows the average envelope curves of the two types of walls. The curves are clustered by wall configurations (there were 5 wall configurations in the experimental study). Also, it shows the drift associated with the start of the uplift of the end-studs in A-walls, denoted as δ_R (see Table 1). In general, the A-walls have greater lateral forces than the C-walls. For the 1200 mm and 3600 mm long specimens, the displacements associated with the maximum lateral force and with the ultimate lateral force are smaller for the A-walls. In the 2400 mm long walls these displacements are similar for the two types of tests. The δ_R limit appears to mark a change in the behavior of the A-walls. This is noticeable on the A240-05-01 specimen in which a change in the tangent-stiffness of the envelope curve is evident.

Fig. 15 shows the degradation of the cyclic effective secant-stiffness, K_{eff} (as defined in Eq. (3) and Fig. 6), calculated for the total lateral displacement of the top plate relative to the base plate. The effective stiffness of A-walls is greater than those of C-walls. For the 1200 mm and 2400 mm long specimens, the A-walls' effective stiffness degrades faster than for C-walls, then, the stiffness values for the two sets of walls converge as the number of cycles (and the lateral deformation) increases. Such effect is less noticeable in 3600 mm long walls.

To compare the cyclic parameters (effective stiffness, dissipated energy, and equivalent viscous damping) at different levels of deformation, Table 3 shows the average values of the ratio between the parameters of the A-walls to those of the C-walls at three levels of drift (1%, 2%, and 3%). These values of drift correspond to the three performance levels (immediate operation IO, life safety LS, and collapse prevention CP) proposed by FEMA 356 [36]. The effect of the axial load in the increase of effective secant-stiffness is larger for the walls with nail-spacing of 50 mm than for the walls with nail-spacing of 100 mm. For the walls with

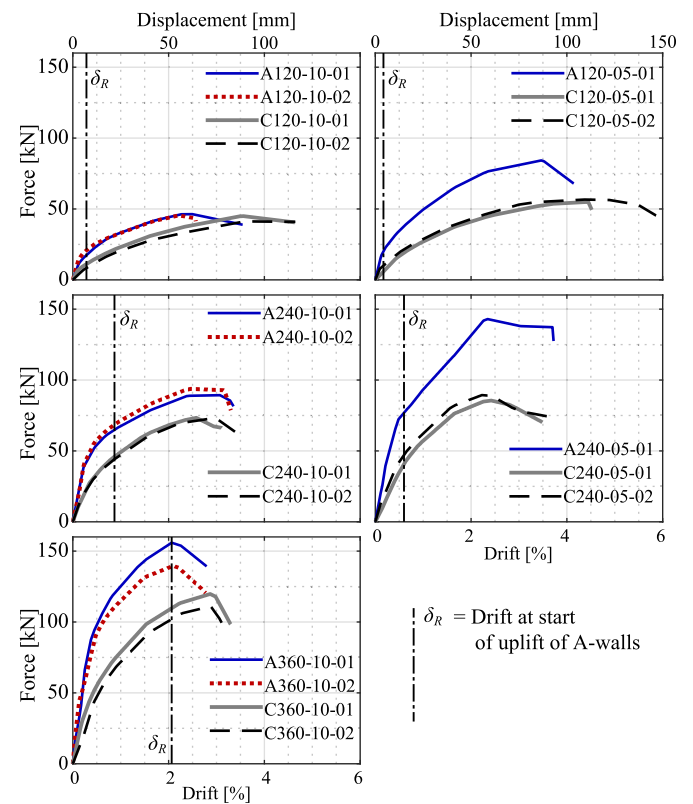


Fig. 14. Comparison of envelope curves of walls tested with compressive load and bending moment (A-walls) and walls tested without compressive load nor bending moment (C-walls) [22].

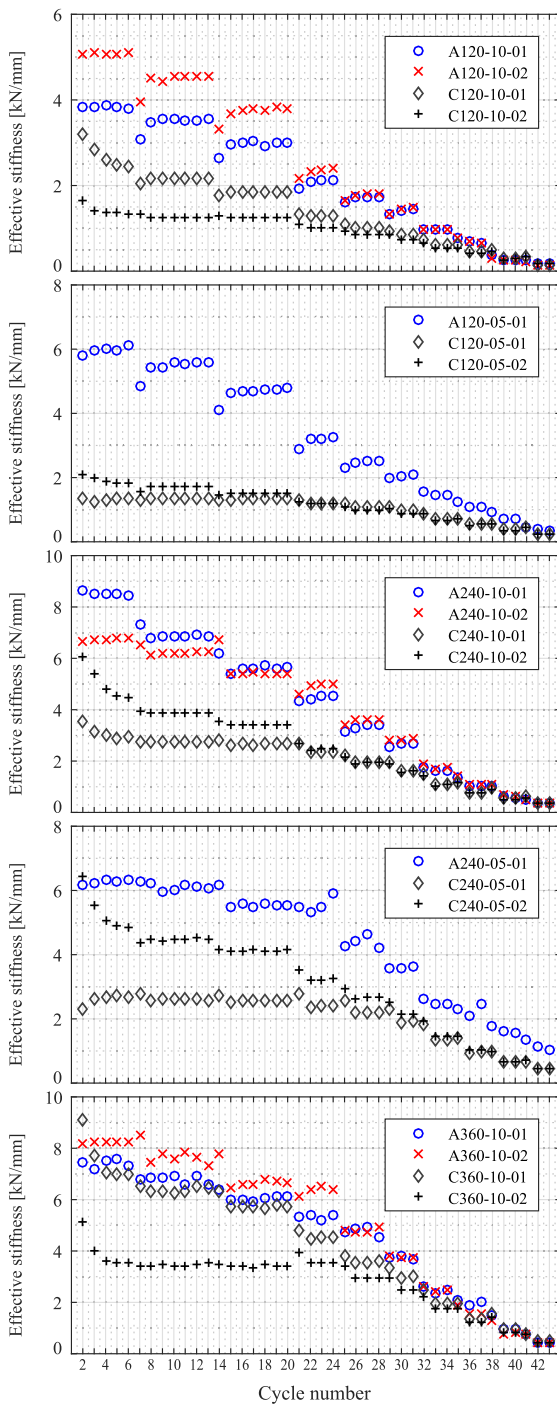


Fig. 15. Effective cyclic stiffness, K_{eff} (see Fig. 6), for the tests (A-walls and C-walls [22]).

Table 3
Ratio (A-walls to C-walls) of the cyclic parameters for different levels of drift, δ .

Wall Configuration	K_{eff} [ratio A/C]			E_d [ratio A/C]			ξ_e [ratio A/C]		
	$\delta = 1\%$	2%	3%	$\delta = 1\%$	2%	3%	$\delta = 1\%$	2%	3%
120-10	1.66	1.40	0.93	4.41	3.13	2.86	2.51	2.16	2.96
120-05	2.08	1.93	1.77	6.69	3.98	3.92	3.22	2.12	2.23
240-10	1.39	1.24	0.95	3.21	3.06	2.69	2.12	2.28	2.70
240-05	1.68	2.39	1.97	3.05	3.17	2.52	1.67	1.35	1.29
360-10	1.27	1.22	0.94	3.40	3.05	3.20	1.71	1.92	2.82

nail-spacing of 100 mm, there are average ratios of 1.44, 1.29, and 0.94 at drifts of 1%, 2%, and 3%; respectively. Then, at the third performance level, the A-walls with nail-spacing of 100 mm show less stiffness than the corresponding C-walls. In contrast, walls with nail-spacing of 50 mm, maintain stiffness ratios greater than 1.0 at the three performance levels.

Fig. 16 shows the dissipated energy per cycle, E_d , calculated as the area enclosed by the hysteresis loops of the total lateral displacement. This shows that A-walls had greater dissipation capacity for all the hysteresis loops. For two consecutive secondary cycles (i.e., cycles with the same displacement amplitude) the dissipated energy decreases slightly. This trend may be due to a change in the coefficient of friction between the components with slip contact. Table 3 shows the ratios of the energy dissipated by a hysteresis loop for the A-walls to the C-walls, at three levels of drift. For the first (IO) and second (LS) performance levels, the energy dissipated per cycle by the A-walls was more than 3-times the energy dissipated by the C-walls. At the third performance level, the ratios range from 2.5 to 3.9.

Fig. 17 shows the equivalent viscous damping per cycle, ξ_e (Eq. (1)), for the hysteresis loops of the total lateral displacement. The values of EVD for the A-walls are greater than those of the C-walls for all the cycles. In Table 3, the values of the ratio of the EVD of the A-walls to the EVD of the C-walls range from 1.67 to 3.22 at the first performance level. These ratios decrease for the second and third performance levels, to between 1.35 and 2.96. No clear trend is observed in the values of these ratios at different drift levels.

3.3. Results of the numerical analysis of the 5-story building

The better performance observed for wood-frame walls under high CL and BM is expected to have a relevant influence on the seismic behavior of mid-rise buildings. Even though it is a common practice to consider the effects of vertical loads when designing and analyzing other structural systems (for instance, by means of the interaction diagram for reinforced-concrete structures), there is no standard procedure to do so for wood-frame buildings. Understanding such effects would be of great relevance to optimize the design of timber buildings. Therefore, this section aims at providing a glance of the lateral performance of wood-frame structures when the effects of the combined action of vertical and lateral loads on the walls are considered. To achieve this goal, static and dynamic analyses were performed for a 5-story wood-frame building. The structure was numerically represented with two nonlinear models (A-model and C-model) as described in Section 2.7.

Static pushover analyses were conducted employing both models. Fig. 18 shows the obtained monotonic pushover curves for both models and each analysis-direction (X-axis and Y-axis). The vertical loads increase the capacity of the building by 56.6% and 46.1% in the X and Y directions, respectively, a result that is consistent with those observed from the wall tests. The initial stiffness of the structure increases by 25.9% and 15.4% for each direction, which results in a reduction of the fundamental period of the building from 0.68 s to 0.64 s. As additional information, the design spectral accelerations, according to the NCh433 [23] regulations, are 0.36 g for the C-model and 0.40 g for the A-model (an increase of 11%). Also, Fig. 18 shows an increase in the lateral displacement capacity and the ductility of the building. This is due to a

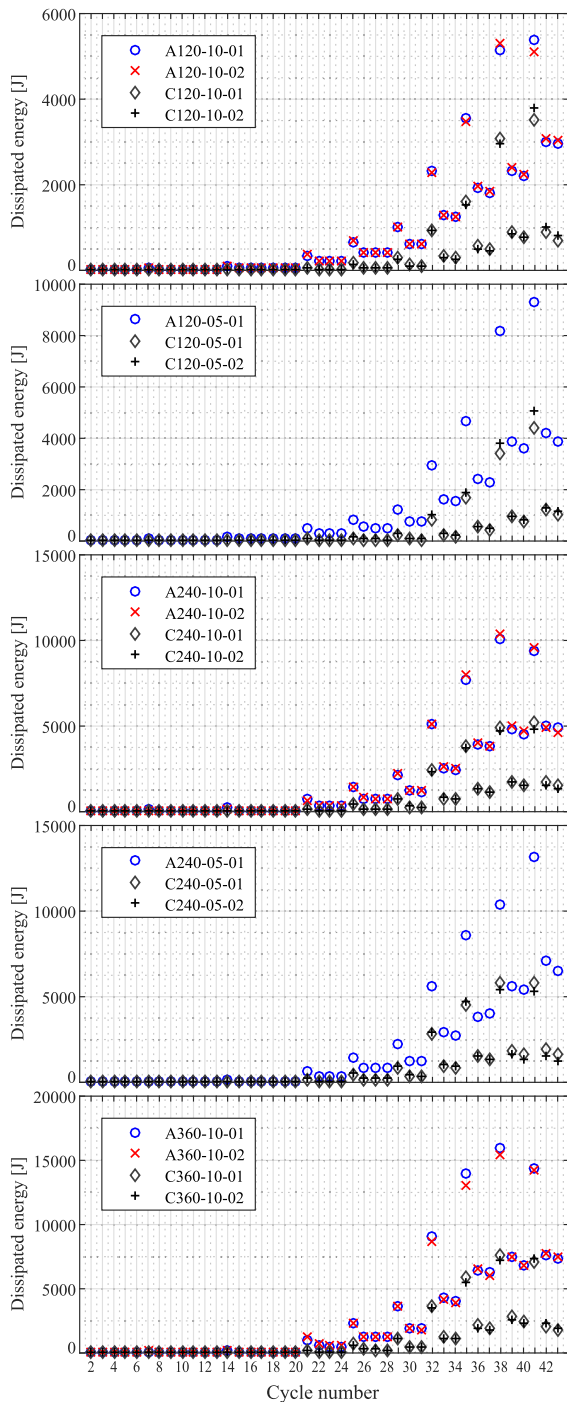


Fig. 16. Dissipated energy per cycle, E_d (see Fig. 6), for the tests (A-walls and C-walls [22]).

higher contribution of the upper stories to the roof displacement when only in the lower stories the effects of the vertical loads are considered. Therefore, such increased ductility does not represent a higher nonlinear deformation capacity of the structure.

Fig. 19 shows the maximum inter-story drifts calculated in the time-history analysis for each story at the center of mass of the floor. For comparison, the three performance levels (immediate operation IO, life safety LS, and collapse prevention CP) proposed by FEMA 356 [36] are also included. Smaller drifts for almost all stories were observed for the model with vertical loads, with a significant improvement in the behavior of the first two stories. In the A-model the third story had the maximum deformation (0.95% drift), which is a consequence of the

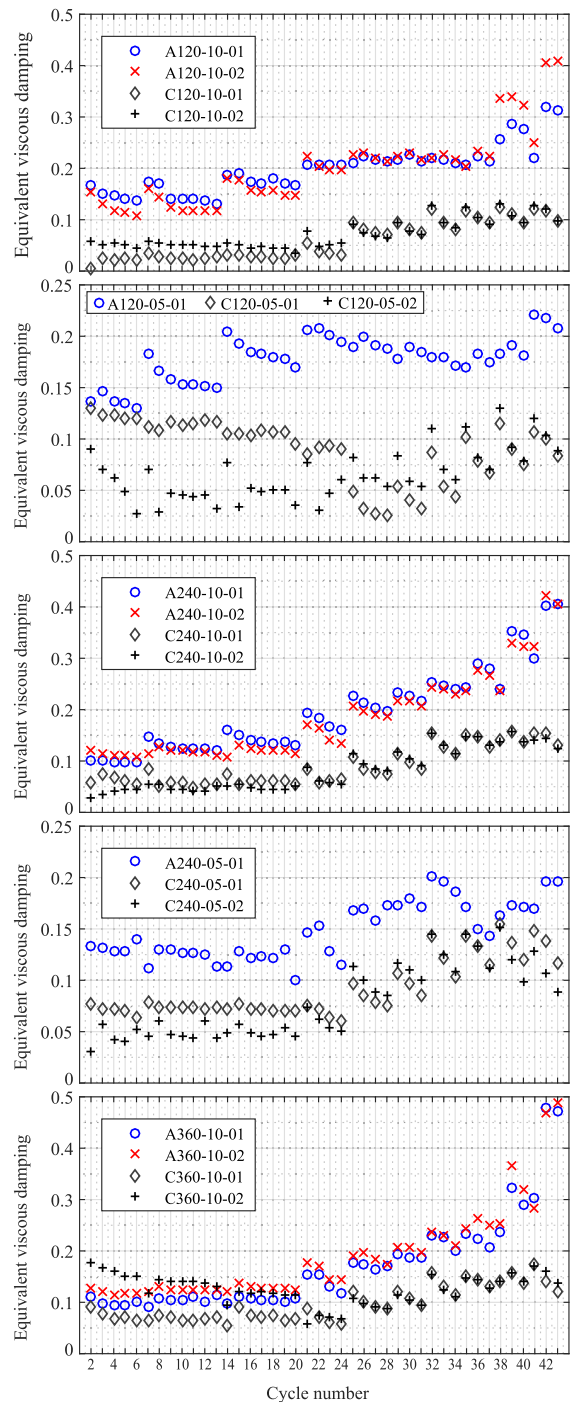


Fig. 17. Equivalent viscous damping (EVD) per cycle (see Fig. 6), for the tests (A-walls and C-walls [22]).

higher stiffness of the lower stories. Incorporating the vertical load effects in the analysis allows accomplishing the IO performance level in all the stories. This highlights the importance of developing a standard methodology to properly incorporate the vertical load effects for performance-based seismic design procedures.

Finally, an incremental dynamic analysis (IDA) [31] was conducted to analyze the response of both models when facing several earthquakes with different dynamic properties. Fig. 20(a) and (b) show the 52 IDA results for each model as well as the collapse capacities computed for a 3% inter-story drift (i.e., the average spectral acceleration at collapse limit). Results show an increase from 1.09 g to 1.30 g (19.3%) in the average collapse capacity when the vertical load effects are considered.

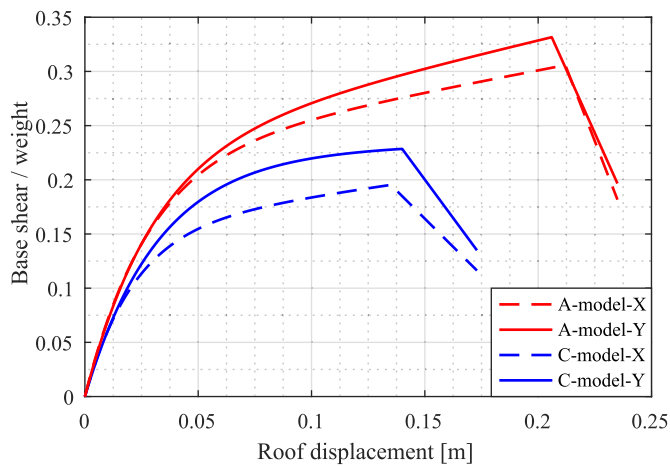


Fig. 18. Pushover results for building models.

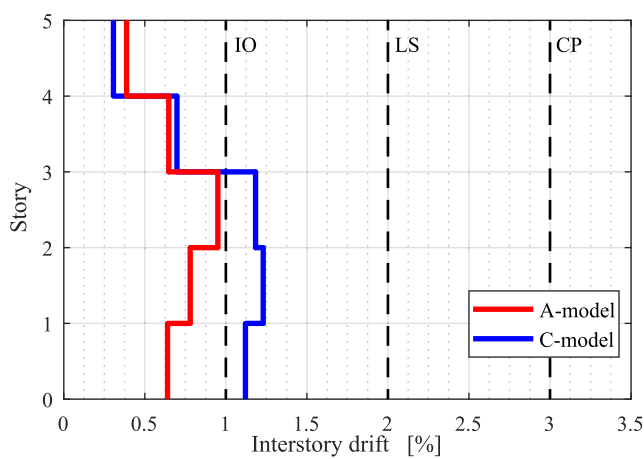
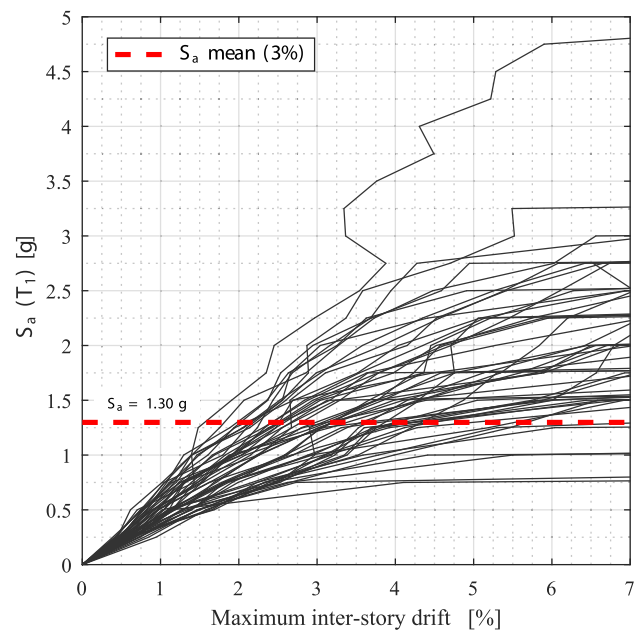


Fig. 19. Maximum inter-story drifts, at the floor's center of mass, recorded from the bi-directional time-history analysis of the building models, subjected to the ground motion of the Maule earthquake (Angol station [30]).

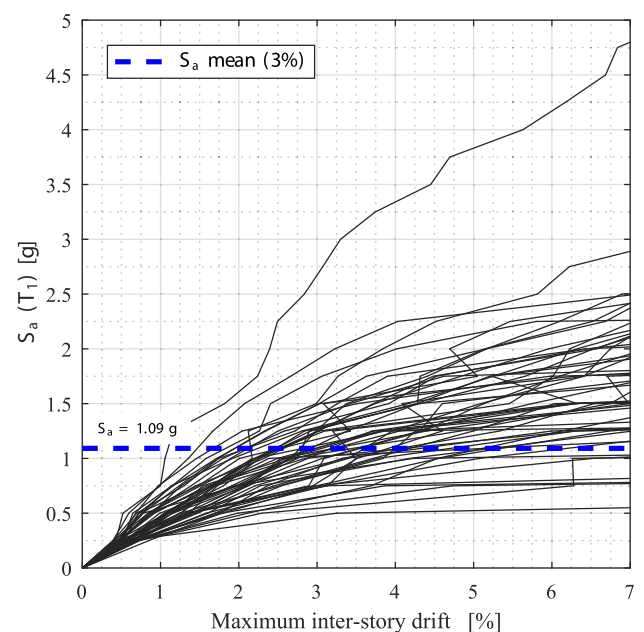
Additionally, a detailed analysis of the results showed that if the improved performance of the lower stories is considered, the damage is evenly distributed on all floors, avoiding a soft-story failure mode in most of the cases. The Collapse Margin Ratio (CMR) is defined as the ratio between the collapse capacity computed from an IDA analysis and the spectral acceleration corresponding to the code-defined Maximum Considered Earthquake (MCE). The NCh2745 standard [37] defines the MCE as 1.5 times the design spectral acceleration. Therefore, the CMRs for the models without and with vertical loads are 2.02 and 2.17, an increase of 7.3% when the vertical loads were considered into the numerical model.

4. Conclusions

This paper presents the results of an experimental investigation conducted to characterize the cyclic lateral behavior of wood-frame shear walls for mid-rise timber buildings. The studied walls had a configuration designed to resist large axial compressive load (CL) and in-plane bending moment (BM) and were cyclically tested in realistic loading conditions (i.e., applying CL and BM). For such walls and loading conditions, few experimental information is available in the literature. An improvement in the lateral behavior was observed compared to walls tested without CL nor BM. To evaluate the effects of this improved wall-behavior on the seismic response of mid-rise timber buildings, a numerical study was performed on a structural model of a 5-



(a) IDA, A-model



(b) IDA, C-model

Fig. 20. Incremental dynamic analysis (IDA) results and collapse capacities for: (a) model with vertical load -A-model-, and (b) model without vertical load -C-model-.

story structure designed according to the Chilean seismic code. Such study showed that the prediction of the structural response is conservative when the numerical model does not consider the effects of the vertical loads. The main observations and conclusions obtained of this research are:

- The observed failure modes of the shear walls subjected to axial CL and in-plane BM are similar to the ones observed in common light wood-frame shear walls tested without compressive load nor bending moment. The main observed damage was local crushing of the wood and nail failure in the panel to frame connections.

- The maximum load-carrying capacity increases as the wall length increases (showing a proportionality trend) or as the panel-edge nail spacing decreases (showing an increase by up to 76%). The initial stiffness increases as the wall length increases and no effect of the nail spacing is observed on this parameter. As the nail spacing decreases, the ductility ratio decreases and the ultimate displacement increases. Similar to observations in a previous study on walls tested without CL, no clear trend is evidenced with respect to the effect of the wall length on the ductility ratio.
- The nominal load-carrying capacity estimated with the Special Design Provisions for Wind and Seismic (SDPWS) underestimates the actual capacity of walls when there are high compressive loads and bending moments on the walls. The load-carrying capacity of the tested walls reached between 1.55- and 1.85-times the nominal capacity estimated according to the SDPWS. Also, the SDPWS expression for the elastic deflection underestimates the actual stiffness of the analyzed walls. The initial stiffness of the tested walls were 1.02- to 1.85-times the SDPWS-based estimation.
- The axial compressive load and bending moment cause an increase in the maximum lateral load-carrying capacity, lateral stiffness, dissipation capacity, and ductility ratio of walls compared to walls tested without CL nor BM. The observed average increase was 37% (ranging from 8 to 63%) for the load-carrying capacity, 141% (ranging from 103 to 191%) for the initial stiffness, 104% (ranging from 36 to 156%) for the representative equivalent viscous damping, and 55% (ranging from 22 to 87%) for the ductility ratio. The improvement in the response parameters suggests that there are changes in both the hysteretic behavior of the panel-to-frame connections and the framing members' interaction. The shape of the hysteresis loops suggests that an as yet non-identified inner frictional phenomenon is the main reason for the increase in the dissipation capacity. These hypotheses are currently being investigated.
- Results from a numerical analysis on a 5-story wood-frame building model showed that high vertical loads might have a relevant impact on the lateral behavior of mid-rise structures and not considering it might be too conservative. The effects of the gravitational loads on the first- and second-story walls modified the dynamic properties of the building, decreasing the fundamental period by 6.7%. Static pushover analyses show that the vertical loads increase the capacity of the building by 51.4% (on average) and the initial stiffness by 20.7%. Also, a greater ductility was obtained when the vertical loads were considered. Dynamic analyses showed that when the vertical loads are considered, the behavior of the structure improves and the inter-story drifts decrease, allowing to achieve the performance levels required to guarantee the resilience of the analyzed building. Besides, an incremental dynamic analysis showed a 19.3% increase in the collapse capacity of the building and a 7.3% increase in the collapse margin ratio, when several ground motions with different characteristics were employed.
- The numerical study shows that to consider the effects of axial compressive load and bending moment in the lateral behavior of wood-frame shear walls could generate better estimates of seismic demands. This is because a correct estimation of the building's lateral stiffness leads to a better calculation of the natural periods and natural vibration modes of the structure. More efficient designs of mid-rise buildings could be achieved by considering the effects of high axial compressive load and bending moment on the lateral response of wood-frame shear walls.

The results of the numerical study highlight the importance of developing a standard methodology to properly incorporate the effects of CL and BM for multi-story timber building design. The acquired data and experience from the experimental study allow calibrating numerical models to predict the seismic behavior of mid-rise timber buildings. The correct characterization of the wall behavior, under more realistic loading conditions, could be used in performance-based seismic design

procedures, which require a detailed description of the force-deformation behavior of individual structural components.

Declaration of Competing Interest

The authors declare that they have no known competing financial interests or personal relationships that could have appeared to influence the work reported in this paper.

Acknowledgments

The research presented in this paper was funded by project 16BPE-62260, CORFO, and the UC Timber Innovation Center (CIM UC), and supported by the Research Center for Integrated Disaster Risk Management (CIGIDEN), ANID/FONDAP/15110017. The shear wall tests were conducted at the Laboratory of Structural Engineering of the Pontificia Universidad Católica de Chile. The first author recognizes the financial support provided by the postgraduate scholarship program of the SEN-ESCYT from the Republic of Ecuador.

References

- [1] Gupta AK, Kuo GP. *J Struct Eng* 1985;111(8):1722–33. [https://doi.org/10.1061/\(ASCE\)0733-9445\(1985\)111:8\(1722\)](https://doi.org/10.1061/(ASCE)0733-9445(1985)111:8(1722)).
- [2] van de Lindt JW. *Pract Period Struct Des Construct* 2004;9(1):44–53. [https://doi.org/10.1061/\(ASCE\)1084-0680\(2004\)9:1\(44\)](https://doi.org/10.1061/(ASCE)1084-0680(2004)9:1(44)).
- [3] Lam F, Filiatrault A, Kawai N, Nakajima S, Yamaguchi N. Performance of timber buildings under seismic load. Part 1: experimental studies. *Prog Struct Mat Eng* 2002;4(3):276–85. <https://doi.org/10.1002/pse.121>.
- [4] Ellingwood BR, Rosowsky DV, Pang W. *J Struct Eng* 2008;134(8):1353–63. [https://doi.org/10.1061/\(ASCE\)0733-9445\(2008\)134:8\(1353\)](https://doi.org/10.1061/(ASCE)0733-9445(2008)134:8(1353)).
- [5] Rose J. Preliminary testing of wood structural panel shear walls under cyclic (reversed) loading. Tech. Rep. 158, APA The Engineered Wood Association (1998). URL http://bayarearetrofit.com/PDFs/APA_Cyclic_Shear_Wall_Testing.pdf.
- [6] Kirkham WJ, Gupta R, Miller TH. *J Struct Eng* 2014;140(4):04013097. [https://doi.org/10.1061/\(ASCE\)ST.1943-541X.0000861](https://doi.org/10.1061/(ASCE)ST.1943-541X.0000861).
- [7] American Wood Council, Wood Frame Construction Manual for One- and Two-Family Dwellings, American National Standards Institute; 2018.
- [8] Salenikovich A, Payeur M. Influence of vertical loads on lateral resistance of light-frame shear walls. In: 11th World Conference on Timber Engineering 2010, WCTE 2010, Vol. 3; 2010.
- [9] Gatto K, Uang C-M. Cyclic response of woodframe shearwalls : loading protocol and rate of loading effects. Tech. Rep. W-13, California Institute of Technology (2002). URL www.curee.org/publications/woodframe/w13.html.
- [10] Pei S, van de Lindt JW, Pryor SE, Shimizu H, Isoda H, Rammer D. Seismic testing of a full-scale mid-rise building : the NEESWood capstone test, Tech. Rep. 10-0008, NEESWood (2010). URL <http://www.buffalo.edu/mceer/catalog/host.html/content/shared/www/mceer/publications/MCEER-10-0008.detail.html>.
- [11] Tomasi R, Sartori T, Casagrande D, Piazza M. Shaking table testing of a full-scale prefabricated three-story timber-frame building. *J Earthquake Eng* 2015;19(3):505–34. <https://doi.org/10.1080/13632469.2014.974291>.
- [12] A. Filiatrault, Woodframe Project Testing and Analysis Literature Reviews , Tech. Rep. W-03, California Institute of Technology (2001). URL www.curee.org/publications/woodframe/w03.html.
- [13] van de Lindt JW, Pei S, Pryor SE, Shimizu H, Isoda H. *J Struct Eng* 2010;136(10):1262–72. [https://doi.org/10.1061/\(ASCE\)ST.1943-541X.0000222](https://doi.org/10.1061/(ASCE)ST.1943-541X.0000222).
- [14] Dean PK, Shenton HW. *J Struct Eng* 2005;131(7):1104–13. [https://doi.org/10.1061/\(ASCE\)0733-9445\(2005\)131:7\(1104\)](https://doi.org/10.1061/(ASCE)0733-9445(2005)131:7(1104)).
- [15] Johnston AR, Dean PK, Shenton HW. *J Struct Eng* 2006;132(9):1426–34. [https://doi.org/10.1061/\(ASCE\)0733-9445\(2006\)132:9\(1426\)](https://doi.org/10.1061/(ASCE)0733-9445(2006)132:9(1426)).
- [16] Grossi P, Sartori T, Tomasi R. Tests on timber frame walls under in-plane forces: part 1 , Proceedings of the Institution of Civil Engineers - Structures and Buildings 168 (11) (2015) 826–839. doi:10.1680/stbu.13.00107.
- [17] Grossi P, Sartori T, Tomasi R. Tests on timber frame walls under in-plane forces: part 2 , Proceedings of the Institution of Civil Engineers - Structures and Buildings 168 (11) (2015) 840–852. doi:10.1680/stbu.13.00108.
- [18] Sadeghi Marzaleh A, Nerbano S, Sebastiani Croce A, Steiger R. OSB sheathed light-frame timber shear walls with strong anchorage subjected to vertical load, bending moment, and monotonic lateral load. *Eng Struct* 173 (March) (2018) 787–799. doi: 10.1016/j.engstruct.2018.05.044.
- [19] Instituto Nacional de Normalización, NCh 1198. Madera - Construcciones en Madera - Cálculo (2014).
- [20] Krawinkler H, Parisi F, Ibarra L, Ayoub A, Medina R. Development of a Testing Protocol for Woodframe Structures. Tech. Rep. W-02, California Institute of Technology (2001). URL www.curee.org/publications/woodframe/w02.html.
- [21] American Society for Testing and Materials, ASTM E2126-11. Standard Test Methods for Cyclic (Reversed) Load Test for Shear Resistance of Vertical Elements of the Lateral Force Resisting Systems for Buildings (2011). URL <https://www.astm.org/Standards/E2126.htm>.

- [22] Guñez F, Santa María H, Almazán JL. Monotonic and cyclic behaviour of wood frame shear walls for mid-height timber buildings, *Engineering Structures* 189 (March) (2019) 100–110. doi:10.1016/j.engstruct.2019.03.043.
- [23] Instituto Nacional de Normalización, NCh 433-96 Mod2009. *Diseño Sísmico de Edificios*; 2009.
- [24] Chopra AK. *Dynamics of Structures Theory and Applications to Earthquake Engineering*. 4th ed. Pearson Education/Prentice Hall; 2012.
- [25] American Wood Council, Special Design Provisions for Wind and Seismic (SDPWS), American National Standards Institute; 2015.
- [26] Nassani DE. A simple model for calculating the fundamental period of vibration in steel structures. *APCBEE Procedia* 9 (June 2014) (2014) 339–346. doi:10.1016/j.apcbee.2014.01.060.
- [27] Folz B, Filiatrault A. *Journal of Structural Engineering* 127 (4) (2001) 433–441. doi: 10.1061/(ASCE)0733-9445(2001)127:4(433).
- [28] Pei S, van de Lindt JW. Coupled shear-bending formulation for seismic analysis of stacked wood shear wall systems. *Earthquake Eng Struct Dyn* 2009;38(14): 1631–47. <https://doi.org/10.1002/eqe.926>.
- [29] Estrella X, Guindos P, Almazán JL, Malek S. Efficient nonlinear modeling of strong wood frame shear walls for mid-rise buildings. *Eng Struct* 2020;215:110670. <https://doi.org/10.1016/j.engstruct.2020.110670>. <https://linkinghub.elsevier.com/retrieve/pii/S014102961933576X>.
- [30] University of Chile, Earthquakes of Chile . URL <http://terremotos.ing.uchile.cl/registros/164>.
- [31] Vamvatsikos D, Allin Cornell C. Incremental dynamic analysis. *Earthquake Engineering and Structural Dynamics* 31 (3) (2002) 491–514. doi:10.1002/eqe.141.
- [32] Estrella X, Guindos P, Almazán JL. Ground motions for FEMA P-695 application in subduction zones. *Latin Am J Solids Struct* 695.
- [33] Lam F, Prion HGL, He M. *J Struct Eng* 123 (12) (1997) 1666-1673. doi:10.1061/(ASCE)0733-9445(1997)123:12(1666).
- [34] Shenton HW, Dinehart DW, Elliott TE. Stiffness and energy degradation of wood frame shear walls. *Can J Civ Eng* 1998;25(3):412–23.
- [35] Jayamon JR, Line P, Charney FA. *J Struct Eng* 2018;144(12):03118003. [https://doi.org/10.1061/\(ASCE\)ST.1943-541X.0002212](https://doi.org/10.1061/(ASCE)ST.1943-541X.0002212).
- [36] FEMA, FEMA 356: Prestandard and Commentary for the Seismic Rehabilitation of Buildings. Tech. rep., Federal Emergency Management Agency, Washington, D. C. (2000). URL <http://sharif.edu/~ahmadizadeh/courses/strcontrol/CIE626-2-FEMA-356.pdf>.
- [37] Instituto Nacional de Normalización, NCh 2745-2013. *Análisis y Diseño de Edificios con Aislación Sísmica*; 2013.